Deep Noisy-Label Learning Based Cross-Resolution Land-Cover Mapping in Kenya

Yinhe Liu[1], Yingxin Wu[2], Faith Karanja[3], Xian Xu[1], Mark K. Boitt[4], Ruiyi Yang[1], Petri Pellikka[5], Yanfei Zhong[1]

[1] State Key Laboratory of Information Engineering in Surveying, Mapping and Remote Sensing, Wuhan University, Wuhan 430079, China
[2] School of Remote Sensing and Information Engineering, Wuhan University, Wuhan 430079, China
[3] Department of Geospatial and Space Technology, University of Nairobi, Nairobi P.O. Box 30197-00100, Kenya
[4] Institute of Geomatics, GIS and Remote Sensing, Dedan Kimathi University of Technology, Private Bag, Dedan Kimathi, Nyeri P.O. Box 10143-10100, Kenya
[5] Department of Geosciences and Geography, University of Helsinki, 00014 Helsinki, Finland

Keywords: Land-cover mapping, noisy-label learning, cross-resolution, deep learning.

Abstract

High-resolution land-cover information is critical for environmental monitoring across rapidly changing African landscapes, yet national-scale 10 m mapping remains limited by scarce training data and inconsistencies among existing products. This study presents a scalable framework for generating a 10 m land-cover map of Kenya for 2022 by integrating multi-temporal Sentinel-2 composites, historical land-cover datasets, and volunteered geographic information. A confidence-weighted fusion of GlobeLand30, FROM-GLC, and FROM-GLC10 produces large-scale synthetic labels that reduce temporal misalignment and systematic biases. A ConvNeXt–UPerNet segmentation network trained with a noise-aware bootstrap focal loss effectively captures Kenya's strong multi-scale heterogeneity, from cropland mosaics and rangelands to riparian corridors and expanding urban areas. The resulting map shows clear improvements in spatial coherence and thematic detail over existing 10–30 m products. The proposed approach offers a practical pathway for routine 10 m national mapping in data-sparse regions and provides timely, reliable information for ecological monitoring, agricultural assessment, and sustainable land-use planning in Kenya and East Africa.

1. Introduction

Land cover describes the physical and biological state of the Earth's surface, including cropland, forest, shrubland, grassland, wetland, water bodies, and artificial surfaces (Lambin and Geist 2008). Wall-to-wall land-cover maps derived from remote sensing are fundamental for monitoring deforestation, land degradation, and rapid urban expansion, and they underpin biogeochemical and biodiversity assessments as well as climate modeling (DeFries 2008; Feddema et al. 2005). While early global products were produced at coarse resolutions (300 m–1 km) (Arino et al. 2008; Bartholome and Belward 2005; Friedl et al. 2010; Hansen et al. 2000), finer-resolution (~30 m) maps have become the de facto standard for many scientific and policy applications because they better capture land-cover patterns at human and ecosystem scales (Giri et al. 2013). The availability of free Landsat data since 2008 (Woodcock et al. 2008) has enabled a series of large-area and global datasets, including CORINE for Europe (Büttner 2014), NLCD for the USA (Homer et al. 2015), NLUD-C for China (Zhang et al. 2014), FROM-GLC (Gong et al. 2019; Gong et al. 2017) and GlobeLand30 (Chen et al. 2015). However, many regions of Africa, including Kenya, still lack consistent, up-to-date, and high-resolution national land-cover maps, especially at the emerging 10 m scale enabled by Sentinel-2 and other sensors.

For applications such as forest and wetland conservation, agricultural monitoring, and urban planning in Kenya, both higher spatial resolution and more frequent temporal updates are required (Bontemps et al. 2012; Marsik et al. 2011). Yet increasing spatial resolution dramatically amplifies the cost of manual training-sample collection and expert verification, which remains a major bottleneck for updating national land-cover products. Conventional model-driven classifiers such as support vector machines (SVM) and random forests (RF) depend heavily on manually engineered features and struggle to efficiently exploit massive training sets, limiting accuracy and scalability (Belgiu and Drăguț 2016; Mountrakis et al. 2011). Hence, many authoritative products (e.g., GlobeLand30, CORINE) still rely on labor-intensive, knowledge-based interactive editing to correct automated results, making regular 10 m updates across large territories such as Kenya difficult and costly (Egorov et al. 2015; Pflugmacher et al. 2019). Deep learning, particularly convolutional neural networks (CNNs), offers automatic feature learning that more closely mimics human visual interpretation and has achieved strong performance in remote-sensing image analysis (Ma et al. 2019), but these data-driven methods are typically constrained by the availability and quality of labeled training data.

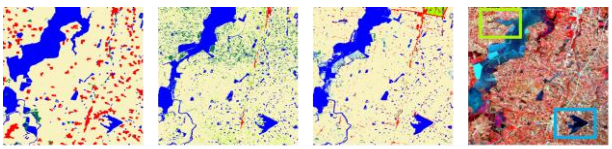

Figure 1 An example of inconsistency between the historical products and the latest image.

An emerging solution is to reuse and transform existing land-cover products as large-scale training labels. Prior work has shown that previously collected samples and historical products can remain effective for new mapping epochs, even when a substantial fraction of labels is imperfect, and that migrated samples based on spectral similarity can achieve accuracy comparable to original labels (Gong et al. 2019; Huang et al. 2020).

However, there are still some problems that need to be solved. Firstly, as shown in Figure 1 (a), (b) and (c), it has been found that the inconsistency among the land-cover maps is more significant than the actual land-cover change (Fritz et al. 2011; Pouliot et al. 2014). This makes it is easy to introduce unavoidable system bias errors when using only a single data

source as the training labels. Secondly, despite the products themselves are consistent, there may by temporal misalignment between the land-cover map and actual image caused by the expansion or shrinkage of the land cover objects (green box in (d)). More serious, for the newly emerged land-cover changes (blue box in (d)), the training labels would contain unavoidable errors even if all the products are correct.

However, directly using a single historical product as training data can introduce substantial systematic biases, because inconsistencies among products often exceed the magnitude of true land-cover change (Fritz et al. 2011; Pouliot et al. 2014). In addition, temporal misalignment between historical maps and contemporary imagery leads to mismatched labels in areas of expansion or shrinkage, and to inevitable errors over newly emerged land-cover types. Finally, traditional SVM/RF-based workflows are not well suited to incremental learning from billions of noisy labels, nor to fully exploiting spatial context at 10 m resolution.

In this study, we adapt a historical-product data-driven deep learning land-cover mapping (HDLC) framework to produce a nationally consistent 10 m land-cover map of Kenya for the year 2022. Multiple historical and existing land-cover products are fused to generate large-scale training labels, whose spatial and spectral relationships to 10 m satellite imagery are explicitly modeled to mitigate temporal inconsistencies and product disagreements. A fully convolutional CNN architecture, derived from the U-Net family with residual connections, is employed to perform efficient end-to-end feature extraction and 10 m land-cover classification over the entire territory of Kenya. To cope with label noise inherent in product-derived training data, we further incorporate label-uncertainty modeling into the training process, using mixture distributions to identify and adaptively correct highly uncertain pixels while preserving reliable labels.

2. Study aera and materials

2.1 Study area

Kenya was selected as the study area because it encompasses a pronounced gradient of bioclimatic and ecological conditions within a relatively compact territory. From the humid, intensively cultivated highlands of central and western Kenya to the semi-arid and arid rangelands of the north and east, and from the Afro-montane forests of Mt. Kenya and the Aberdare Range to the coastal mosaics of mangroves, croplands, and urban areas along the Indian Ocean, the country hosts most of the major terrestrial land-cover types in tropical Africa. In addition, extensive inland water bodies such as Lake Victoria, Lake Turkana, and numerous smaller lakes and wetlands contribute to a highly heterogeneous landscape. Over recent decades, Kenya has experienced rapid population growth, agricultural expansion, infrastructure development, and localized deforestation and urbanization, particularly around Nairobi and other major towns. These dynamics make Kenya an ideal testbed for developing and evaluating 10 m land-cover mapping methods that must capture both fine-scale fragmentation and rapid land-cover transitions.

2.2 Existing global land-cover products

To support the generation of the 10 m land-cover map of Kenya for 2022, we made use of several existing global land-cover products at 30 m and 10 m resolutions as historical reference and auxiliary information:

GlobeLand30 (Chen et al. 2015): GlobeLand30 is a 30 m global land-cover product produced by the National Geomatics Center of China for the years 2000 and 2010, with 10 land-cover classes. Independent validation studies have reported overall accuracies on the order of 80% at the global scale. In this study, the GlobeLand30 maps were used as a coarse-resolution reference layer to provide prior information on the spatial distribution of major land-cover types in Kenya, and as one of the historical products contributing to pseudo-label generation.

FROM-GLC-2015 (Gong et al. 2017): FROM-GLC-2015 is the second generation of the Finer Resolution Observation and Monitoring of Global Land Cover (FROM-GLC) dataset (Li et al. 2017), produced at 30 m resolution for circa 2015 using automated supervised classification of multi-season Landsat 8 imagery and all-season land-cover samples. We employed FROM-GLC-2015 as an independent 30 m benchmark over Kenya and as an additional historical product in the fusion of training labels, thereby increasing the robustness of the label ensemble in regions where individual products disagree.

FROM-GLC10 (Gong et al. 2019): FROM-GLC10 is the first 10 m global land-cover product, generated for 2017 by transferring a 30 m sample set collected in 2015 to Sentinel-2 imagery. In this work, FROM-GLC10 plays a dual role. First, it serves as a prior 10 m land-cover layer for Kenya that guides the design of the national legend and supports consistency with existing global products. Second, it is incorporated into the historical-product ensemble used to construct large-scale 10 m pseudo-labels for training the 2022 Kenya-specific classifier.

By jointly exploiting these products, we leverage complementary information from multiple epochs and sensors, while explicitly modeling and mitigating the inter-product inconsistencies and temporal mismatches that are known to exceed true land-cover changes in many regions (Fritz et al., 2011; Pouliot et al., 2014).

2.3 Auxiliary data

OpenStreetMap (OSM) (Haklay and Weber 2008) was used as an important source of ancillary vector information to refine class delineation and to provide additional training and validation cues, particularly for artificial surfaces and transportation infrastructure. OSM is one of the most successful volunteered geographic information projects, in which contributors digitize and update features such as roads, buildings, water bodies, and land-use polygons using GPS tracks, field observations, or aerial and satellite imagery. The resulting geospatial database is freely available in multiple formats and has been demonstrated to be a reliable supervised information source for land-cover classification in various regions (Johnson and Iizuka 2016).

For Kenya, most OSM layers (e.g., roads, residential areas, industrial zones, airports, ports, and major water bodies) were downloaded from Geofabrik (http://download.geofabrik.de) in shapefile format. However, the directly downloaded data primarily contain the core attributes of each feature and may not fully capture local environmental dynamics. For instance, ephemeral pans, seasonal wetlands, or intermittently flowing rivers in arid and semi-arid lands can be tagged as “water” although they are dry for large parts of the year. To better distinguish such features, we exploited the “seasonal” and related tags to filter OSM entities that exhibit strong seasonal variability. Structured SQL queries were constructed and executed via the Humanitarian OpenStreetMap Team (HOT) export tools (https://export.hotosm.org) to selectively retrieve features with specific combinations of tags relevant for land-cover classification in Kenya (e.g., permanent vs. seasonal water, major vs. minor roads, residential vs. industrial built-up areas). The resulting OSM layers were rasterized and

harmonized with the 10 m grid to support both training-label refinement and post-classification editing.

2.4 Validation dataset

The independent validation dataset for Kenya was derived from and extended beyond existing crowdsourced land-cover samples collected within the framework of the Geo-Wiki project (https://www.geo-wiki.org/) (Fritz et al. 2009; Fritz et al. 2017). Geo-Wiki volunteers visually interpret very high resolution imagery to assign land-cover labels at predefined sample locations, and these crowdsourced data have been widely used to validate global products such as FROM-GLC. In this study, we first extracted all Geo-Wiki samples falling within the national boundaries of Kenya and mapped their original classes to the land-cover legend adopted for the 10 m 2022 Kenya product. When multiple volunteers provided conflicting labels at the same location, a majority voting scheme was applied to derive the most likely class. To ensure spatial independence and avoid over-representation of particular areas, dense clusters of points associated with targeted campaigns were thinned based on a minimum-distance criterion, thereby approximating a more random and unbiased spatial sampling.

The resulting crowdsourced sample set was then systematically reviewed and augmented through expert visual interpretation. High-resolution Google Earth imagery and multi-season Sentinel-2 images centered on 2022 were used to check and, where necessary, correct existing labels, and to add new samples in underrepresented land-cover types and eco-regions (e.g., montane forests, coastal mangroves, irrigated agriculture, and semi-arid rangelands). Particular attention was paid to regions undergoing rapid change, such as peri-urban areas around Nairobi, Mombasa, Kisumu, and major infrastructure corridors. The final validation dataset, stratified by land-cover class and Kenya's main ecological zones, provides an independent benchmark for assessing the accuracy and class-specific performance of the 10 m 2022 Kenya land-cover map.

3. Methodology

3.1 Land-cover mapping framework

3.1.1 Overview of the proposed method: The overall workflow for producing the 10 m land-cover map of Kenya for 2022 is illustrated in Fig. 3. The framework comprises three main components. First, all available Sentinel-2 images over Kenya for the year 2022 are acquired and preprocessed on the Google Earth Engine (GEE) platform (Gorelick et al. 2017) to generate temporally robust, cloud-free 10 m composites. Second, existing global land-cover products and auxiliary geospatial datasets (including OSM) are integrated to synthesize large-scale training samples tailored to Kenyan land-cover conditions. Third, a modified semantic segmentation network based on a fully convolutional residual U-Net is trained on these synthetic samples and applied in an end-to-end manner to derive the final 10 m land-cover map for Kenya.

This design explicitly exploits the synergy between multi-temporal 10 m imagery, multi-source historical products, and a deep learning architecture capable of learning spatial–spectral context across highly heterogeneous Kenyan landscapes, ranging from densely cultivated highlands to arid rangelands and rapidly expanding urban regions.

3.1.2 Multi-temporal image composite: In equatorial East Africa, persistent cloud cover over the highlands and Lake Victoria basin, together with strong intra-annual phenological dynamics (e.g., during the long and short rainy seasons), complicates the direct use of single-date imagery for national-scale mapping. Even when individual cloud-free scenes are available, large radiometric and phenological differences between acquisition dates can introduce spatial inconsistencies that degrade classification performance at the national scale.

To mitigate these effects, we constructed a multi-temporal, cloud-free Sentinel-2 composite for the year 2022. All Sentinel-2 Level-2A images over Kenya with a reported cloud cover <30% were retrieved from GEE. For each image, cloud and cloud-shadow pixels were identified using the quality assessment bands and an additional cloud index, and masked according to a conservative threshold. For every 10 m band, the remaining (non-cloudy) observations over 2022 were aggregated on a pixel-by-pixel basis, and the median value was computed to form a robust annual composite. This median composite effectively suppresses residual cloud contamination, reduces the influence of outliers, and integrates phenological information from multiple seasons while preserving the spatial resolution required to resolve fine-scale field patterns and urban morphology.

All compositing operations were implemented in GEE (Gorelick et al. 2017), a planetary-scale geospatial cloud computing platform that provides direct access to global archives of satellite imagery (e.g., MODIS, Landsat, Sentinel) and scalable parallel processing. GEE was therefore used to streamline image selection, cloud masking, compositing, and reprojection to a common 10 m grid covering the entire territory of Kenya.

3.1.3 Multi-source sample synthesis: Supervised land-cover classification requires representative and accurate training samples for each class. At national or continental scales, manual selection and labeling of training data is extremely labor-intensive and often dominates the overall cost of mapping (Pflugmacher et al. 2019). At the same time, the proportion of land area undergoing annual change is relatively small compared to the total extent, even in rapidly transforming landscapes, which makes existing land-cover products a valuable source of reusable training information.

In this study, we treated several existing global products as primary label sources and fused them with auxiliary vector data to generate synthetic training samples for Kenya. Following the legends of GlobeLand30 and FROM-GLC (Chen et al., 2015; Gong et al., 2017, 2019), we adopted a 10-class classification system: cropland, forest, grassland, shrubland, wetland, water bodies, artificial surfaces (built-up areas), bare land, snow/ice,

Land-cover class	OSM tags
Farmland	land-use = farmland
Forest	land-use = forest
Grass	land-use = grass; land-use=meadow
shrubland	natural = scrub; natural = heath
Wetland	land-use = wetland; natural = mud
Water	waterway = river; natural = water
Tundra	natural = tundra
Impervious	land-use = industrial; land-use = railway; highway = ∗; land-use = commercial; land-use = retail; land-use = residential;
Bare land	natural = sand; natural=bare_rock
Snow&Ice	natural=glacier

Table 1. Mapping between the used classification system and the corresponding OSM tags

and tundra. For equatorial Kenya, tundra does not occur and snow/ice is restricted to very small patches on high mountain peaks; these classes were retained in the legend for consistency with global products but are negligible in area in our study region. All input land-cover products were reprojected to WGS 1984 and resampled to the common 10 m grid via interpolation and rasterization.

Let L denote the set of historical land-cover maps used for fusion. For each land-cover map L, we denote by $p^L i, j(c)$ the probability (or indicator) that pixel (i, j) belongs to class c, and by w_L the confidence weight assigned to product L. Because direct per-pixel confidence information is not available, w_L was approximated using the user's accuracy of each product reported in previous validation studies (Chen et al., 2015; Brovelli et al., 2015; Yang et al., 2017; Gong et al., 2019). The fused synthetic label Si, j at pixel (i, j) is obtained by weighted combination and normalization:

$$S_{i,j}(c) = \sum_L w_L, p^L i, j(c) / \sum L w_L \qquad (1)$$

where $S_{i,j}(c)$ is the normalized class probability for class c. The final class label for (i, j) is given by the maximum-probability class in $S_{i,j}$, optionally subject to additional consistency checks. This multi-product fusion reduces the impact of systematic biases and inconsistencies associated with any single product (Fritz et al., 2011; Pouliot et al., 2014).

To further refine class boundaries, especially for artificial surfaces and transportation infrastructure, we incorporated OpenStreetMap (OSM) data (Haklay and Weber, 2008). After downloading the relevant OSM layers for Kenya from Geofabrik and HOT Export (Johnson and Iizuka, 2016; Liu et al., 2020), linear features (e.g., roads, railways, rivers) and polygonal features (e.g., residential areas, industrial zones, water bodies, forests, wetlands) were rasterized onto the 10 m grid. These features were then mapped to the adopted land-cover classes using the tag–class correspondence in Table 1. The OSM-derived land-cover layer was stacked above the fused products, so that OSM information overrides the historical products where reliable volunteered geographic information is available.

3.2 Deep land cover classification network

3.2.1 land-cover classification model structure: To fully exploit the spatial–spectral information in the 10 m Sentinel-2 composite and the dense synthetic labels, we adopt a semantic segmentation framework that couples a ConvNeXt backbone with a UPerNet decoder. A four-stage ConvNeXt processes 10 m Sentinel-2 tiles and produces hierarchical feature maps at progressively coarser resolutions, capturing local texture (e.g., smallholder plots and informal settlements), intermediate patterns (e.g., plantation blocks, urban blocks), and broad ecological context (e.g., transitions from highland cropland to semi-arid rangelands). UPerNet applies a pyramid pooling module to the deepest feature map to encode global scene context, and then fuses multi-level features through a top-down feature pyramid with lateral connections, yielding a high-resolution feature map from which a final convolution and softmax layer produce per-pixel class probabilities for the Kenyan 10-class legend. This ConvNeXt–UPerNet design is well suited to Kenya's strong multi-scale heterogeneity, enabling coherent delineation of extensive cropland and rangeland while preserving narrow and fragmented features such as riparian corridors, roads, and coastal fringes.

3.2.2 Model training with noise- and imbalance-aware loss: The network is trained end-to-end using a bootstrap focal (BF) loss that is simultaneously robust to noisy pseudo-labels and class imbalance:

$$\ell_{\mathrm{BF}} = -\sum_{i=1}^{C} (1 - p_i)^{\gamma} \left((1 - w_i) y_i + w_i z_i\right)^{\top} \log(p_i) \qquad (2)$$

where C is the number of land-cover classes, p_i is the softmax probability vector for class i, y_i is the one-hot encoded pseudo-label, z_i is the current model prediction, w_i is a class-specific reliability weight derived from historical user's accuracies, and γ is the focusing parameter. This loss down-weights easy, well-classified pixels, emphasizes hard and minority-class examples, and adaptively balances trust between historical product labels and the model's own predictions, leading to a more robust 10 m 2022 Kenya land-cover map.

To fully exploit the spatial–spectral information in the 10 m Sentinel-2 composite and the dense synthetic labels, we adopt a semantic segmentation framework that couples a ConvNeXt backbone with a UPerNet decoder. A four-stage ConvNeXt processes 10 m Sentinel-2 tiles and produces hierarchical feature maps at progressively coarser resolutions, capturing local texture (e.g., smallholder plots and informal settlements), intermediate patterns (e.g., plantation blocks, urban blocks), and broad ecological context (e.g., transitions from highland cropland to semi-arid rangelands). UPerNet applies a pyramid pooling module to the deepest feature map to encode global scene context, and then fuses multi-level features through a top-down feature pyramid with lateral connections, yielding a high-resolution feature map from which a final 1×1 convolution and softmax layer produce per-pixel class probabilities for the Kenyan 10-class legend. This ConvNeXt–UPerNet design is well suited to Kenya's strong multi-scale heterogeneity, enabling coherent delineation of extensive cropland and rangeland while preserving narrow and fragmented features such as riparian corridors, roads, and coastal fringes.

The network is trained end-to-end using a bootstrap focal loss that is simultaneously robust to noisy pseudo-labels and class imbalance:

Input imagery comprises all Sentinel-2 Level-2A scenes acquired between 1 January and 31 December 2022. After removing cloud and cirrus pixels with the Sen2Cor probability band, a per-pixel median composite is generated and re-projected to a 10 m grid, producing a seasonally neutral, cloud-free mosaic.

Initial labels are formed by reprojecting GlobeLand30-2020 into eight management-relevant classes. To counter jagged edges, a super-resolution conditional random field (SR-CRF) aligns coarse masks to Sentinel-2 gradients. The SR-CRF outputs soft probabilities that better match high-resolution object geometry.

Network architecture adopts a dual-path high-resolution design: a context branch captures broad semantic patterns through progressive down-sampling, while a detail branch preserves native geometry via invertible blocks. A mutual-attention module at each stage computes query–key interactions between branches, allowing fine edges to inherit coherent context without post-hoc interpolation.

Noise mitigation uses a compact class-conditional label-correction scheme. During an initial warm-up, per-pixel cross-

entropy losses are logged and modelled—separately for every class—by a two-component Beta mixture. Pixels with high posterior probability of being erroneous receive greater reliance on the network's own prediction inside a soft-bootstrap objective; trusted pixels continue to follow the historical label.

4. Results

Examples from the training dataset are shown in Figure 2, where it can be seen that the generated annotations have good consistency with the corresponding images, which could thus be used as training data to drive the learning of the deep model. More importantly, the process of generating samples is fully automatic, so that the scale of the dataset is very large, which can fully satisfy the training of the data-hungry FCN model.

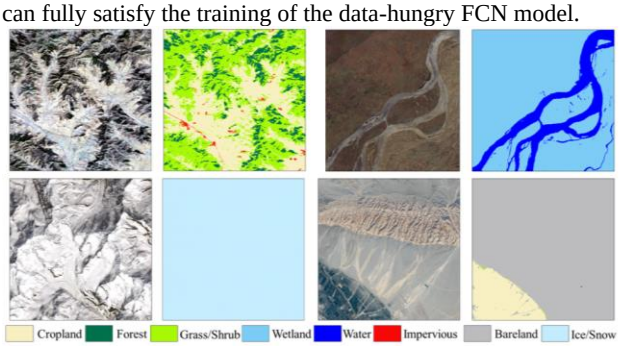

Figure 2 Examples of generated land cover classification training labels.

Although the FCN has no requirements on the size of the input image, it can perform end-to-end pixel-to-pixel classification for images of any size. However, limited by the hardware, it is unrealistic to directly classify the billions of pixels in the entire remote sensing image. Therefore, the study area was divided uniformly into mapsheets of dimensions 4◦ in longitude and 3◦ in latitude to facilitate the data organization and processing. In the border of each mapsheet, the input image is symmetrically padded to supplement spatial context information, so as to ensure that there is no obvious break between the mapsheets. Although the image is cropped into numerous mapsheets, it is still unrealistic to predict the entire image directly. The images need to be cropped into sub-image patches of a certain size and input into the model to perform land cover classification. To ensure that the prediction results between patches are consistent, there is a certain overlap between patches when sampling patches. The predicted probabilities at the overlap between patches are averaged and all the patches are stitched into an entire image as the final classification result.

Visual assessment shows pronounced improvements over the resampled 30 m masks: river channels are continuous, tea-plantation terraces in Kericho emerge clearly, and peri-urban expansion around Nairobi is delineated with parcel-level fidelity. The mutual-attention backbone retains narrow linear features that a plain HRNet blurs, while adaptive noise weighting suppresses salt-and-pepper artefacts in minority classes such as wetlands. Expert reviewers confirm that mangrove and irrigated-cropland extents align well with field knowledge. Although a full accuracy audit is ongoing, spot checks indicate clear gains over ESA WorldCover 2021 and the unrefined historical masks.

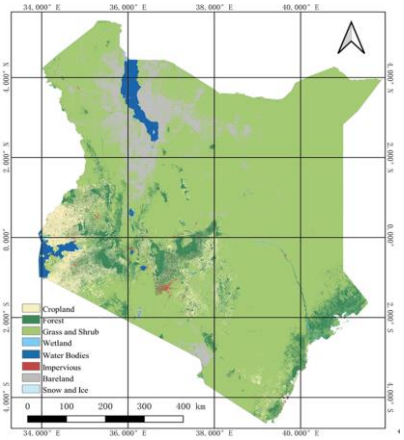

Figure 3 10-m Resolution land cover map of Kenya.

5. Conclusion

This study presents a scalable framework for generating a nationally consistent 10 m land-cover map of Kenya for 2022 by integrating multi-temporal Sentinel-2 imagery, multi-source historical land-cover products, and volunteered geographic information within a noise-aware deep learning architecture. By fusing GlobeLand30, FROM-GLC, and FROM-GLC10 into confidence-weighted synthetic labels and training a ConvNeXt–UPerNet segmentation model with a robust bootstrap focal loss, the method overcomes persistent challenges of label scarcity, inter-product inconsistencies, and fine-scale landscape fragmentation. The resulting map exhibits substantial improvements in spatial coherence and thematic detail over both 30 m products and existing global 10 m datasets, accurately depicting heterogeneous Kenyan landscapes—from highland agriculture and montane forests to arid rangelands and expanding urban areas. The framework offers a practical, fully automated solution for regular 10 m national updates in data-limited regions and provides a reliable foundation for environmental monitoring, agricultural management, and sustainable development planning in Kenya and across East Africa.

6. Acknowledgements

This study was supported by the National Key Research and Development Program of China and Shandong Province, China,under Grant 2021YFB3901300.

References

Arino, O., Bicheron, P., Achard, F., Latham, J., Witt, R., & Weber, J.-L. (2008). The most detailed portrait of Earth. *Eur. Space Agency*, *136*, 25–31-25–31

Bartholome, E., & Belward, A.S. (2005). GLC2000: a new approach to global land cover mapping from Earth observation data. *International Journal of Remote Sensing*, *26*, 1959–1977-1959–1977

Belgiu, M., & Drăguţ, L. (2016). Random forest in remote sensing: A review of applications and future directions. *ISPRS Journal of Photogrammetry and Remote Sensing*, *114*, 24–31-24–31

Bontemps, S., Herold, M., Kooistra, L., Groenestijn, A.v., Hartley, A., Arino, O., Moreau, I., & Defourny, P. (2012). Revisiting land cover observation to address the needs of the climate modeling community. *Biogeosciences*, *9*, 2145–2157-2145–2157

Büttner, G. (2014). CORINE Land Cover and Land Cover Change Products. In I. Manakos, & M. Braun (Eds.), *Land Use and Land Cover Mapping in Europe: Practices & Trends* (pp. 55-74). Dordrecht: Springer Netherlands

Chen, J., Chen, J., Liao, A., Cao, X., Chen, L., Chen, X., He, C., Han, G., Peng, S., Lu, M., & others (2015). Global land cover mapping at 30 m resolution: A POK-based operational approach. *ISPRS Journal of Photogrammetry and Remote Sensing*, *103*, 7–27-27–27

DeFries, R. (2008). Terrestrial vegetation in the coupled human-earth system: contributions of remote sensing. *Annual Review of Environment and Resources*, *33*, 369–390-369–390

Egorov, A.V., Hansen, M.C., Roy, D.P., Kommareddy, A., & Potapov, P.V. (2015). Image interpretation-guided supervised classification using nested segmentation. *Remote sensing of environment*, *165*, 135-147

Feddema, J.J., Oleson, K.W., Bonan, G.B., Mearns, L.O., Buja, L.E., Meehl, G.A., & Washington, W.M. (2005). The importance of land-cover change in simulating future climates. *Science*, *310*, 1674–1678-1674–1678

Friedl, M.A., Sulla-Menashe, D., Tan, B., Schneider, A., Ramankutty, N., Sibley, A., & Huang, X. (2010). MODIS Collection 5 global land cover: Algorithm refinements and characterization of new datasets. *Remote sensing of environment*, *114*, 168–182-168–182

Fritz, S., McCallum, I., Schill, C., Perger, C., Grillmayer, R., Achard, F., Kraxner, F., & Obersteiner, M. (2009). Geo-Wiki. Org: The use of crowdsourcing to improve global land cover. *Remote Sensing*, *1*, 345–354-345–354

Fritz, S., See, L., McCallum, I., Schill, C., Obersteiner, M., Van der Velde, M., Boettcher, H., Havlík, P., & Achard, F. (2011). Highlighting continued uncertainty in global land cover maps for the user community. *Environmental Research Letters*, *6*, 044005-044005

Fritz, S., See, L., Perger, C., McCallum, I., Schill, C., Schepaschenko, D., Duerauer, M., Karner, M., Dresel, C., Laso-Bayas, J.-C., & others (2017). A global dataset of crowdsourced land cover and land use reference data. *Scientific data*, *4*, 170075-170075

Giri, C., Pengra, B., Long, J., & Loveland, T.R. (2013). Next generation of global land cover characterization, mapping, and monitoring. *International Journal of Applied Earth Observation and Geoinformation*, *25*, 30–37-30–37

Gong, P., Liu, H., Zhang, M., Li, C., Wang, J., Huang, H., Clinton, N., Ji, L., Li, W., Bai, Y., & others (2019). Stable classification with limited sample: transferring a 30-m resolution sample set collected in 2015 to mapping 10-m resolution global land cover in 2017. *Science Bulletin*, *64*, 370–373

Gong, P., Wang, J., Ji, L., & Yu, L. (2017). Landsat Based Land Cover Product for 2015 (FROM-GLC 2015 v0.1). *https://doi.org/10.6084/m9.figshare.5362774.v1*

Gorelick, N., Hancher, M., Dixon, M., Ilyushchenko, S., Thau, D., & Moore, R. (2017). Google Earth Engine: Planetary-scale geospatial analysis for everyone. *Remote sensing of environment*, *202*, 18-27

Haklay, M., & Weber, P. (2008). Openstreetmap: User-generated street maps. *IEEE Pervasive Computing*, *7*, 12–18-12–18

Hansen, M.C., DeFries, R.S., Townshend, J.R.G., & Sohlberg, R. (2000). Global land cover classification at 1 km spatial resolution using a classification tree approach. *International Journal of Remote Sensing*, *21*, 1331–1364-1331–1364

Homer, C.G., Dewitz, J., Yang, L., Jin, S., Danielson, P., Xian, G.Z., Coulston, J., Herold, N., Wickham, J., & Megown, K. (2015). Completion of the 2011 National Land Cover Database for the Conterminous United States – Representing a Decade of Land Cover Change Information. *photogrammetric engineering and remote sensing*, *81*, 345-354

Huang, H., Wang, J., Liu, C., Liang, L., Li, C., & Gong, P. (2020). The migration of training samples towards dynamic global land cover mapping. *ISPRS Journal of Photogrammetry and Remote Sensing*, *161*, 27-36

Johnson, B.A., & Iizuka, K. (2016). Integrating OpenStreetMap crowdsourced data and Landsat time-series imagery for rapid land use/land cover (LULC) mapping: Case study of the Laguna de Bay area of the Philippines. *Applied Geography*, *67*, 140–149-140–149

Lambin, E.F., & Geist, H.J. (2008). *Land-use and land-cover change: local processes and global impacts*. Springer Science & Business Media

Li, C., Gong, P., Wang, J., Zhu, Z., Biging, G.S., Yuan, C., Hu, T., Zhang, H., Wang, Q., Li, X., & others (2017). The first all-season sample set for mapping global land cover with Landsat-8 data. *Science Bulletin*, *62*, 508–515-508–515

Ma, L., Liu, Y., Zhang, X., Ye, Y., Yin, G., & Johnson, B.A. (2019). Deep learning in remote sensing applications: A meta-analysis and review. *ISPRS Journal of Photogrammetry and Remote Sensing*, *152*, 166–177-166–177

Marsik, M., Stevens, F.R., & Southworth, J. (2011). Amazon deforestation: Rates and patterns of land cover change and fragmentation in Pando, northern Bolivia, 1986 to 2005. *Progress in Physical Geography*, *35*, 353–374-353–374

Mountrakis, G., Im, J., & Ogole, C. (2011). Support vector machines in remote sensing: A review. *ISPRS Journal of Photogrammetry and Remote Sensing*, *66*, 247-259

Pflugmacher, D., Rabe, A., Peters, M., & Hostert, P. (2019). Mapping pan-European land cover using Landsat spectral-temporal metrics and the European LUCAS survey. *Remote sensing of environment*, *221*, 583–595-583–595

Pouliot, D., Latifovic, R., Zabcic, N., Guindon, L., & Olthof, I. (2014). Development and assessment of a 250 m spatial resolution MODIS annual land cover time series (2000–2011) for the forest region of Canada derived from change-based updating. *Remote sensing of environment*, *140*, 731-743

Woodcock, C.E., Allen, R., Anderson, M., Belward, A., Bindschadler, R., Cohen, W., Gao, F., Goward, S.N., Helder, D., Helmer, E., & others (2008). Free access to Landsat imagery. *Science*, *320*, 1011–1011-1011–1011

Zhang, Z., Wang, X., Zhao, X., Liu, B., Yi, L., Zuo, L., Wen, Q., Liu, F., Xu, J., & Hu, S.J.R.S.o.E. (2014). A 2010 update of National Land Use/Cover Database of China at 1:100000 scale using medium spatial resolution satellite images, *149*, 142-154